Journal of Power Sources 243 (2013) 472–480

Contents lists available at SciVerse ScienceDirect

Journal of Power Sources

journal homepage: www.elsevier.com/locate/jpowsour

Tungsten materials as durable catalyst supports for fuel cell electrodes

M. Perchthaler [a,*], T. Ossiander [a], V. Juhart [a], J. Mitzel [b], C. Heinzl [c], C. Scheu [c], V. Hacker [d]

[a] Elcomax GmbH, Bayerwaldstrasse 3, 81737 Munich, Germany
[b] Saarland University, Physical Chemistry, 66123 Saarbruecken, Germany
[c] Department of Chemistry, Ludwig-Maximilians-University Munich, Butenandtstr. 11, Gerhard-Ertl-Gebäude, 81377 Munich, Germany
[d] Institute of Chemical Engineering and Environmental Technology, Graz University of Technology, Steyrergasse 21, 8010 Graz, Austria

HIGHLIGHTS

- Tungsten carbide and tungsten oxide were used as catalyst support for HT-PEMFC.
- Tungsten oxide showed higher stability compared to carbon materials.
- 1000 h test of tungsten oxide based anode in HT-PEM stack was done.

ARTICLE INFO

Article history:
Received 7 February 2013
Received in revised form
3 June 2013
Accepted 4 June 2013
Available online 14 June 2013

Keywords:
Tungsten carbide
Tungsten oxide
Catalyst support
High-temperature proton exchange membrane fuel cell

ABSTRACT

Durable platinum catalyst support materials, e.g. tungsten carbide (WC), tungsten oxide (WO_x) and self-synthesized tungsten oxide (WO_{xs}) were evaluated for the use in High-Temperature Proton Exchange Fuel Cells (HT-PEM) based on phosphoric acid doped polybenzimidazole as electrolyte. The support materials and the catalyst loaded support materials were characterized *ex*-situ by cyclic voltammetry in $HClO_4$, potential cycling, CO-stripping, electron microscopy and X-ray diffraction measurements. The tungsten oxide and tungsten carbide based supported catalysts were compared to High Surface Area Carbon (HSAC), each coated with platinum via the same in-house manufacturing procedures. The in-house manufacturing procedures resulted in catalyst particle sizes on HSAC of 3–4 nm with a uniform distribution.

The *in-situ* Potential Cycling experiments of WO_x or WO_{xs} supported catalysts showed much lower degradation rates compared to High Surface Area Carbons. The formation of WO_x species on WC was proven by *ex*- and *in-situ* cyclic voltammetric studies and thermogravimetric analyses. X-ray diffraction, *ex-situ* cyclic voltammetry and *in-situ* cyclic voltammetry showed that WO_x is formed from WC as starting material under oxidizing conditions. Finally a 1000 h durability test with WO_x as catalyst support material on the anode was done in a HT-PEM fuel cell with reformed methanol on the anode.

1. Introduction

The corrosion of today's widely used high surface area carbon blacks is one of the main reasons of performance degradation in fuel cells, especially under start–stop conditions and high electrochemical potentials on anode and cathode. Because of high potentials and temperatures the carbon catalyst support oxidizes to CO_2, which can be detected in the anode and cathode off-gas [1]. A lot of effort was put in the development of more stable carbon compounds as catalyst support material, especially with a more graphitic structure, e.g. carbon nanotubes or carbon nanofibers. These structured carbon materials show lower carbon corrosion rates [2–4], but they cannot prevent carbon oxidation.

Due to this non-carbon materials with high corrosion resistance and high stability under acidic fuel cell conditions are in the focus of interest of research groups worldwide in order to substitute conventional electrode material. However there are several factors which are important for catalyst support materials such as high surface area, porosity, electrical conductivity, electrochemical stability and surface functional groups [5]. These mentioned parameters have to be fulfilled for any successful application.

Tungsten Oxides (WO_x) are compounds with very high melting points of 1700 °C and very low vapor pressure [6]. WO_x is formed by

* Corresponding author.
E-mail addresses: markus.perchthaler@elcomax.com (M. Perchthaler), tanja.ossiander@elcomax.com (T. Ossiander), viktorija.juhart@elcomax.com (V. Juhart), j.mitzel@mx.uni-saarland.de (J. Mitzel), christoph.heinzl@cup.uni-muenchen.de (C. Heinzl), christina.scheu@cup.uni-muenchen.de (C. Scheu), viktor.hacker@tugraz.at (V. Hacker).

0378-7753/$ – see front matter © 2013 Elsevier B.V. All rights reserved.
http://dx.doi.org/10.1016/j.jpowsour.2013.06.022

the reaction of metallic tungsten with oxygen to form stoichiometric tungsten trioxide (WO_3) and lower non stoichiometric oxides WO_x, with $2 < x < 3$ [7]. $WO_{2<x<3}$ is an *n*-type semiconductor with a band gap of about 2.6–2.8 eV [8]. It has a high conductivity which arises from a donor level formed by oxygen-vacancy defects. This leads to the decrease in the resistivity from 1 Ω cm for WO_2 to a minimum of 0.1 Ω cm for $WO_{2.75}$ [8], which is sufficient for the use in fuel cell electrodes.

Hobbs and Tseung [9] observed that the rate for hydrogen oxidation in acidic solution increases by the use of Polytetrafluoroethylene (PTFE) bonded Pt supported on WO_3. They explained this behavior with hydrogen that spills over onto the surface of the hydrogen tungsten bronze (H_xWO_3), freeing these Pt sites for further chemisorptions of hydrogen. This spill-over mechanism of hydrogen between WO_3 and Pt has been suggested as being responsible for the increased activity for the Oxygen Reduction Reaction (ORR) [10]. On the other hand Ota et al. [11] claimed that the observed enhancement of the ORR activity is due to reduced PtO_2 formation. This leads to a higher oxide free Pt-surface area, which is more active for the ORR. Further works on the topic of the relationship between structure and activity of Pt on different synthesized WO_3 support material were done by Shim et al. [12] and Kulesza and Faulkner [13]. They showed that Pt loaded WO_3 nanorods are more stable compared to WO_3 bulk when cycling is conducted between −0.2 and 1.0 V in 2 N H_2SO_4 for several times.

As discussed before WO_3 shows a considerable high proton transfer due to the formation of WO_3 hydrates. This is a very attractive property for fuel cell catalyst supports [14] since this has a beneficial impact on the number of three phase reaction zones, where the catalyst is in contact with an electron conducting support and a proton conducting electrolyte.

In contrast to WO_x, WC was also evaluated as possible material for fuel cell catalyst supports and even catalyst material for the hydrogen oxidation reaction (HOR). Nikolov and Vitanov [15,16] investigated the corrosion resistance of WC in H_2SO_4 and the changes in catalytic activity during corrosion. They discovered that the amount of oxides linearly increases with time, suggesting that during corrosion the catalyst surface was not passivated. In contrast to these findings, Brady et al. [17] reported passivation of WC based catalysts. Depending on the surface stoichiometric ratio of W:C, with higher W content, surface passivation to WO_3 in H_2SO_4 occurs. This causes a loss of electrocatalytic activity of WC for the HOR.

Chhina et al. [18] claimed that the stability of WC under electrochemical oxidizing conditions is higher compared to High Surface Area Carbons (HSAC). Meng and Shen [19–21] studied the effect of the addition of Pt onto WC. They observed a ten times larger activity for the ORR of Pt–W_2C/C than that of Pt/C in an alkali medium and proposed a synergy between W_2C and Pt. In acidic media Santos et al. [22] found that the use of Pt on W_2C as catalyst support material leads to a remarkable enhancement of the ORR activity compared to Pt on carbon, although both catalysts follow the four electron mechanism. Another idea from Shao et al. [23] to get a higher stability of the catalyst support material is to coat the commercial available carbon based catalyst supports with an electrochemical process with phase pure WC and Pt. They achieved a two fold increase of the corrosion resistivity compared to not coated carbon based support materials.

The major drawback of commercial available WC and W_2C is the low Brunauer–Emmett–Teller (BET) surface area (2.1 $m^2\ g^{-1}$) compared to HSAC (about 250 $m^2\ g^{-1}$), which hinders their implementation in fuel cells. Ganesan and Lee [24] synthesized platinum particles on WO_3 nanoparticles with controlled oxidation of W_2C microspheres by calcination at 773 K in O_2 atmosphere for 3 h. Zhu et al. [25] recently showed that the electrochemical stability of WC is dependent on the specific surface area. The higher the specific surface area, the more WC is prone to get oxidized to WO_3 under oxidizing electrochemical conditions (>0.7 V). They also measured very low ORR activity values, which they explained by a high contact resistance between the catalyst and catalyst support. When WC is oxidized it forms an insulating WO_3 layer. This layer blocks the electron transfer between the catalyst and catalyst support, and according to that the contact resistance increases significantly [26].

In this study we evaluate the characteristics of WC, self-made WO_{xs} and commercial available WO_x for the use as electrode material in high-temperature proton exchange (HT-PEM) fuel cells. Electrodes are fabricated with and without platinum and their electrochemical properties are investigated and compared to each other.

The materials are evaluated in *in-situ* experiments in HT-PEM fuel cells and *ex-situ* with Cyclic Voltammetry (CV), Potential Cycling (PC), CO-Stripping, Thermogravimetric Analysis (TGA), X-ray diffraction (XRD) and electron microscopy investigations. The resulting degradation effects, the formation of WO_x and tungsten bronzes and the influence of the catalyst support on the CO-oxidation behavior are discussed. Finally a 980 h long term test at constant load in a HT-PEM fuel cell stack was done and no degradation was observed.

2. Experimental

2.1. Synthesis of WO_{xs}

Commercial available WC (WC CRC 010u, Wolfram Bergbau und Hütten AG) with a BET surface area of 2.71 $m^2\ g^{-1}$ and a grain size of 0.47 μm were oxidized in order to obtain a surface oxidized WO_{xs} species.

For this, the raw WC powder (3 g) is dispersed in 50 ml of a mixture (3:2) of HNO_3 (65 wt%, BDH Prolabo, AnalaR Normapur) and H_2SO_4 (98 wt%, MERCK KGAA, EMSURE) and heated under reflux for 6 h. After this treatment the resulting green powders are washed several times with deionized water until a neutral pH value was obtained.

2.2. Catalyst deposition

The deposition of platinum catalyst on the different catalyst supports is realized via electroless deposition methods. WO_x, WO_{xs}, WC and for comparison HSAC based catalyst supports (0.5 g) are ultrasonicated in a three neck round bottom flask in 30 ml of ethylene glycol and 10 ml deionized water. The deposition of the Pt precursor was done according to the procedure described elsewhere [26]. A platinum loading of 13 wt% on tungsten and HSAC based powders is obtained and confirmed via elemental and Energy-Dispersive X-ray (EDX) measurements.

2.3. Determination of catalyst crystallite size and support structure

To investigate the general morphology and to determine the overall chemical composition of the Pt loaded and unloaded electrode materials a JEOL JSM-6500F scanning electron microscope operated at 4.0 kV and equipped with an energy-dispersive X-ray detector from Oxford Instruments (Inca Energy) was used. Using the implemented JEOL standard detector, secondary electron (SE) images were acquired. SEM top view samples were prepared using conventional preparation techniques. Transmission electron microscopy (TEM) investigations were accomplished by using a FEI Titan 80–300 (S)TEM microscope equipped with a Gatan Tridiem image filter and an EDAX EDX detector for analytical measurements. Standard TEM samples were obtained by suspending the

powders in ethanol (100%) followed by ultrasonication for 10 min and placing it on a holey carbon coated copper grid. The Titan was operated at 300 kV for all measurements.

2.4. Electrochemical characterization

2.4.1. Ex-situ cyclic voltammetry

The electrochemical measurements are performed in a PTFE cell, using a working electrode with a glassy carbon substrate (2.01 cm^2 geometrical surface area) and a potentiostat (Ivium) in a conventional three-electrode setup with an aqueous 0.1 N $HClO_4$ solution. The electrolyte is prepared using deionized water (>17.8 MΩ) and 1 N $HClO_4$ (BDH Prolabo). A chlorine free saturated Hg/Hg_2SO_4 electrode (Radiometer) was used as reference electrode, and a glassy carbon electrode (Radiometer) as counter electrode. All potentials are given to the reversible hydrogen potential.

The catalysts or the catalyst supports are ultrasonically suspended in isopropanol/water. Then an appropriate amount of 42 μg cm^{-2} catalyst support or 7 μg cm^{-2} Pt for catalyst loaded support material are pipetted on the glassy carbon surface and are dried at room temperature to get a uniform film on the glassy carbon electrode.

After immersion into the nitrogen saturated electrolyte the catalyst is treated by potential cycling between 50 and 1100 mV with 500 mV s^{-1} until a stable CV is recorded. The scanning speed in all analysis measurements is set to 50 mV s^{-1}. The analysis scan is performed between 50 mV and 1100 mV.

2.4.2. Potential cycling

PC experiments are done by cycling the catalyst 3600 times at a scan rate of 500 mV s^{-1} between 50 mV and 1100 mV, followed by an analysis scan. Then they are cycled 3600 times between 50 mV and 1200 mV, followed by an analysis scan, and finally 3600 times between 50 mV and 1300 mV followed by an analysis scan. The decrease of the charge in the analysis scans between 50 mV and 400 mV is compared to the starting value and the relative loss is calculated.

2.4.3. CO-stripping

For supported catalysts the electrochemical active surface area (ECA) and the CO-oxidation behavior is measured in an electrochemical cell. The same cell as in the CV measurements is used. The electrolyte is purged for 90 s with a flow of CO (100 mL min^{-1}) at an adsorption potential of 50 mV to obtain a CO monolayer on the catalyst. At this potential the catalyst is blocked very fast with CO. After that the electrolyte is purged with nitrogen for 18 min in order to remove any excess CO from the electrolyte.

The working electrode is then cycled between 50 mV and 1100 mV to get information about the CO-desorption charge, the ECA and the onset potential of the CO oxidation. The ECA is calculated according to equation (1).

$$\mathrm{ECA}\left(\mathrm{m^2\ g^{-1}}\right) = \frac{Q_{CO}}{420 \times 10^{-6}\mathrm{C\ cm^{-2}} \times M} \times 1000 \qquad (1)$$

Q_{CO} is the charge for the CO oxidation on Pt, 420 × 10^{-6} C cm^{-2} is the charge required for the oxidation of a monolayer of adsorbed CO on 1 cm^2 of Pt surface and M is the Pt loading of the electrode.

2.5. Electrode and membrane-electrode-assembly preparation

For *in-situ* tests of the supported catalysts Membrane Electrode Assemblies (MEAs) are prepared and evaluated by *in-situ* CV tests and *in-situ* CO-stripping. The catalyst support is applied on a wet proofed carbon based gas diffusion layer via a doctor blade process.

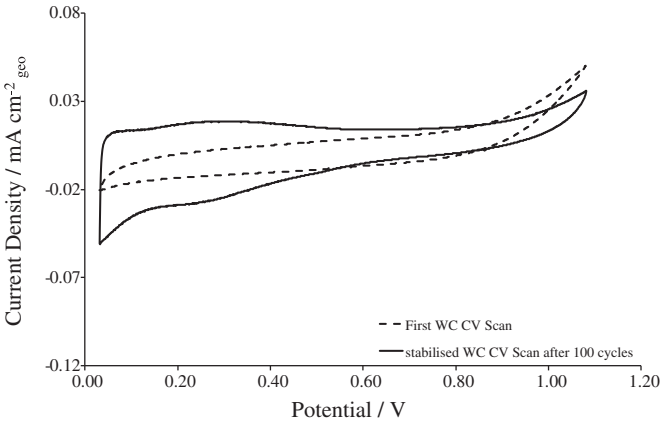

Fig. 1. CV curves of commercially available WC in 0.1 N $HClO_4$ at room temperature and sweep rates of 0.05 V s^{-1} and a loading of 42 μg cm^{-2} before and after stabilization of the CV.

The catalyst support slurry consists of PTFE dispersion (Dyneon™, TF 5035 PTFE), used as hydrophobic reagent and binder, deionized water and isopropanol (gradient grade, Merck). The applied slurry is dried at 170 °C. Then the catalyst is deposited on the catalyst support layer via an electroless deposition method. The HT-PEM MEAs are manufactured by doping the catalyst layer with phosphoric acid and hot pressing them with a membrane based on polybenzimidazole (PBI).

2.6. In-situ test conditions

CVs are recorded in a 50 cm^2 HT-PEM single cell at cell temperatures of 160 °C with humidified nitrogen with a relative humidity of 6% at ambient pressure. The gas flows are 131 mL min^{-1} for H_2 and 100 mL min^{-1} for N_2. The electrochemical measurements are carried out with an electrochemical workstation (Zahner IM6) and a power potentiostat (Zahner PP240). CVs were recorded between 52 mV and 1200 mV with a sweep rate of 50 mV s^{-1} and three cycles per measurement.

2.7. Thermogravimetric analysis

The catalyst support materials are characterized by a thermogravimetric analysis system. The heating rate is set to 10 °C min^{-1}

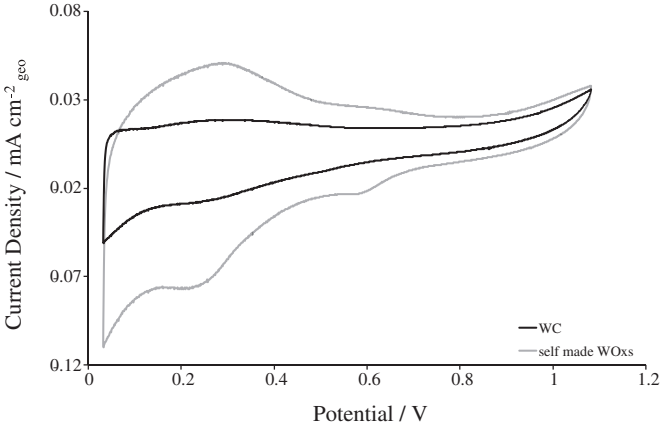

Fig. 2. CV curves of WC and self-made WO_{xs} without platinum in 0.1 N $HClO_4$ at room temperature, sweep rates of 0.05 V s^{-1} and a loading of 42 μg cm^{-2} after 100 potential cycles with 0.5 V s^{-1}.

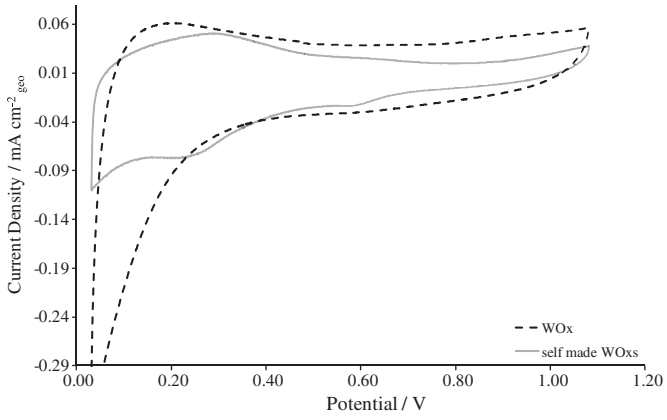

Fig. 3. CV curves scans of commercial WO_x and self-made WO_{xs} in 0.1 N $HClO_4$ at room temperature, sweep rates of 50 mV s^{-1} and a loading of 42 μg cm^{-2}.

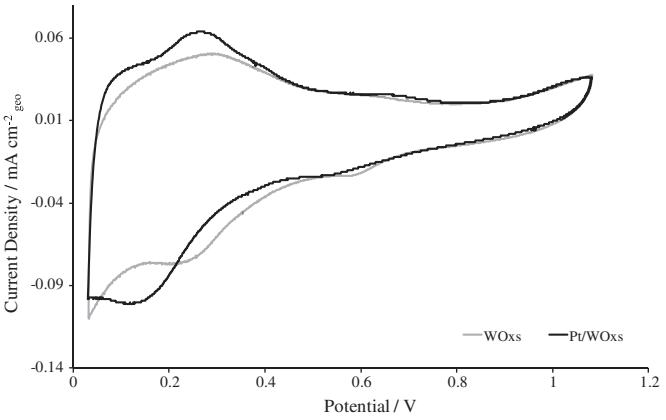

Fig. 5. CV curves of Pt/WO_{xs} and WO_{xs} after stabilization with a sweep rate of 50 mV s^{-1} in 0.1 N $HClO_4$.

starting from 40 °C to 450 °C under air atmosphere. The weight change of the sample (starting weight approx. 10 mg) is recorded.

2.8. HT-PEM long term stack test

The HT-PEM MEAs were tested in a 20-cell stack at a constant current of 0.2 A cm^{-2}. As anode gas reformed methanol with 1.2 vol % CO, 76 H_2 and 22.8% CO_2 was used. The cell potential over the time is recorded.

3. Results and discussion

3.1. Characterization of WC support material

The commercially available WC powders were used as reference and starting material for the WO_x synthesis. In Fig. 1 the CV analysis before and after 100 cycles between 52 mV and 1100 mV are shown.

The first scan shows a significant oxidation current starting at about 0.9 V. This can be attributed to the oxidation of WC and formation of surface oxides. After 100 scans with a sweep rate of 0.5 V s^{-1} the CVs are stabilized and the oxidation currents at potentials higher than 0.9 V are decreased. In addition to that, at lower potentials the shape of the CV changed significantly. After most of the surface is oxidized, WC shows a muted peak between 0.7 and 0.8 V. The surface oxidation of WC–WO_x can be identified with the peak area at low potentials between 0.052 V and 0.4 V in the oxidation and reduction direction of the CV [12,13]. This shape can be assigned to the intercalation of protons into the support material. The applied electrochemical pre-treatment of WC in acidic media and the applied potentials are comparable to the conditions in an operating fuel cell.

3.2. Characterization of self-made WO_{xs}

For the characterization of self-made WO_{xs}, ex-situ CVs of the prepared samples were recorded. The stabilized CV curves after 100 cycles of each material are shown in Fig. 2.

The synthesis of WO_{xs} leads to a more pronounced peak in the potential range which is characteristic for WO_x compared to the WC sample after 100 electrochemical potential cycles. Starting from the same WC material the chemical oxidation leads to a higher level of amorphous or nanoparticulate WO_x as observed in literature [26]. Bearing in mind that mechanical detachment of catalyst from the catalyst support material is a main degradation factor in fuel cell electrodes, the use of WC, which is prone to get oxidized on the surface, is not suitable as support material for fuel cell electrodes.

3.3. Characterization of commercial WO_x

The CV curve of commercially available WO_x (WO_3-XY-JM, Wolfram Bergbau und Hütten AG) with a BET surface area of ~5 m^2 g^{-1} is compared to self-made WO_{xs} (Fig. 3).

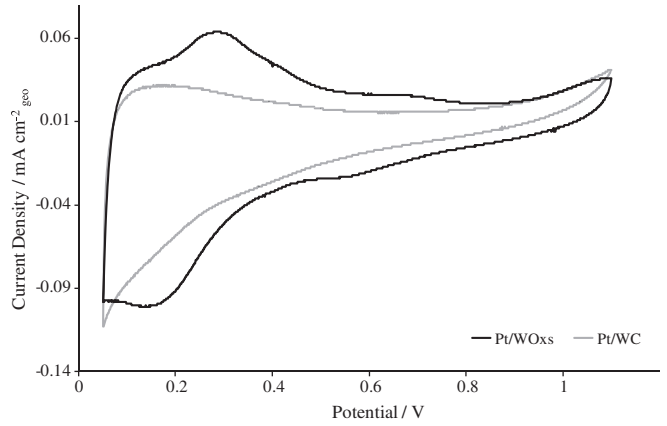

Fig. 4. CV curves of Pt/WC and Pt/WO_{xs} after stabilization with a sweep rate of 0.05 V s^{-1} in 0.1 N $HClO_4$.

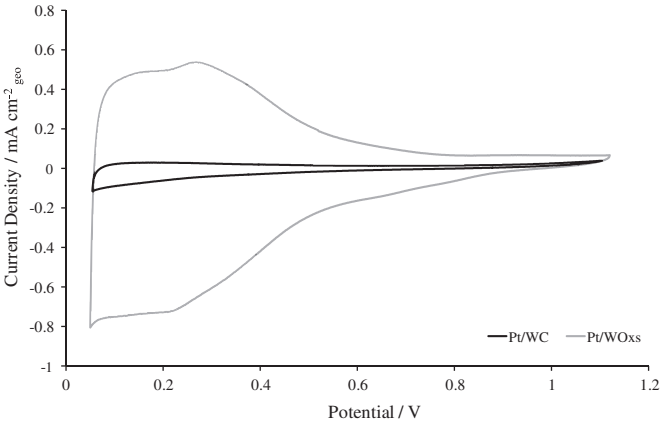

Fig. 6. CV curves of Pt/WC and Pt/WO_{xs} with a sweep rate of 0.05 V s^{-1} in 0.1 N $HClO_4$.

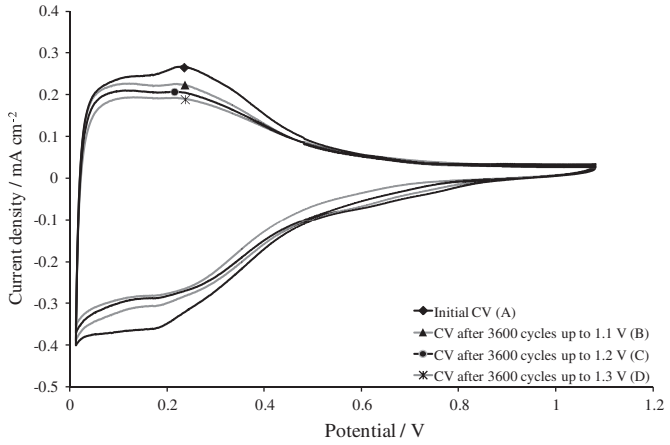

Fig. 7. Analysis scans of WO_x supported Pt catalyst. (A) Initial analysis scan of Pt/WO_x, (B) after 3600 cycles up to 1.1 V, (C) after 3600 consecutive cycles up to 1.2 V and (D) after 3600 consecutive cycles up to 1.3 V.

The commercial WO_x shows a more pronounced current in the WO_x designated low potential region in the oxidation direction, which is comparable to results shown in Fig. 2.

For commercially available WO_x the hydrogen oxidation current increases dramatically compared to WC or WO_{xs} materials. This indicates that the activity of the WO_x samples toward the formation of hydrogen is higher compared to WC or WO_{xs} samples. The BET surface areas of the two samples are comparable within an order of magnitude.

3.4. Catalyst deposition on tungsten based support materials

The CV curves of WO_{xs} and WC catalyst support material after platinum deposition are given in Fig. 4. They possess very different characteristics in the voltammetric profile compared to each other. This is in accordance with the results of the non catalyst loaded supports (see Fig. 2). The self-made Pt/WO_{xs} shows a more pronounced peak area in the WO_x characteristic low potential region compared to Pt/WC, which can be attributed to the formation of tungsten bronzes (compare Equation (2)).

$$WO_3 + xH^+ + xe^- \leftrightarrow H_xWO_3 \quad (2)$$

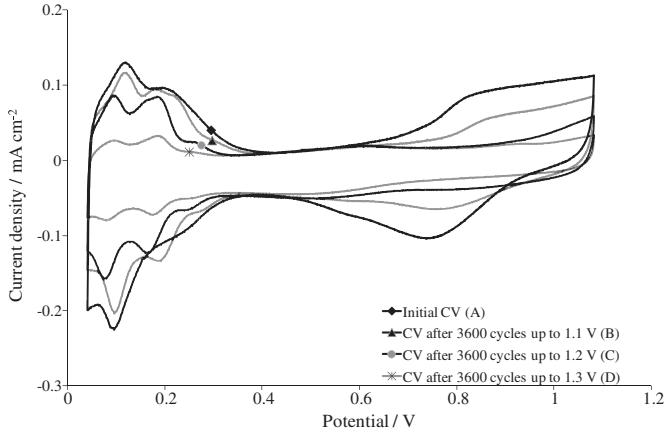

Fig. 8. Analysis scans of Pt loaded HSAC. (A) Initial analysis scan of Pt loaded HSAC, (B) after 3600 cycles up to 1.1 V, (C) after 3600 consecutive cycles up to 1.2 V and (D) after 3600 consecutive cycles up to 1.3 V with a sweep rate of 0.05 V s^{-1} in 0.1 N $HClO_4$.

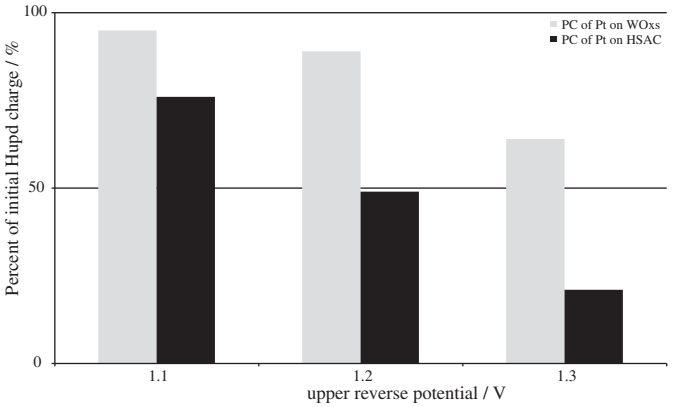

Fig. 9. Comparison of H_{upd} charge loss of different supported Pt catalysts after 3600 cycles with upper reverse potentials of 1.1, 1.2 and 1.3 V.

The CV curve of the Pt/WC sample in Fig. 4 shows the analysis scan after 100 stabilization cycles, where the H_{upd} region gets more pronounced (compare Fig. 1). The Pt/WO_{xs} sample shows a characteristic WO_x behavior in the low potential region even in the first CV cycle.

In Fig. 5 the analysis scans of Pt/WO_{xs} and WO_{xs} are shown. The H_{upd} region of Pt/WO_x shows the same characteristics of Pt in the H_{upd} region. Below 0.4 V several processes occurs: hydrogen underpotential deposition (H_{upd}) and desorption, formation of tungsten bronzes and formation and decomposition of substoichiometric tungsten oxides. So it is not possible to distinguish between these superimposing factors occurring in the low potential region [27].

The formation of oxides on the surface of WC is confirmed by the results of the electrochemical characterization of WO_x. The CV curves of the commercial available WO_x, where Pt is deposited via the same in-house procedure, reveals the same shape compared to self-made WO_{xs}. The CV measurements of Pt/WO_x and Pt/WC are displayed in Fig. 6.

The peak in the low potential region in the case of Pt/WO_x is more than one magnitude higher than for the Pt/WC. The CV shape of Pt/WO_{xs} is similar to the CV shape of WO_x. Another difference is the double layer charge capacity (C_{dl}) in the region of about 0.6 V, which is much higher in the case of Pt/WO_x, which indicates a higher surface area of WO_x compared to WC.

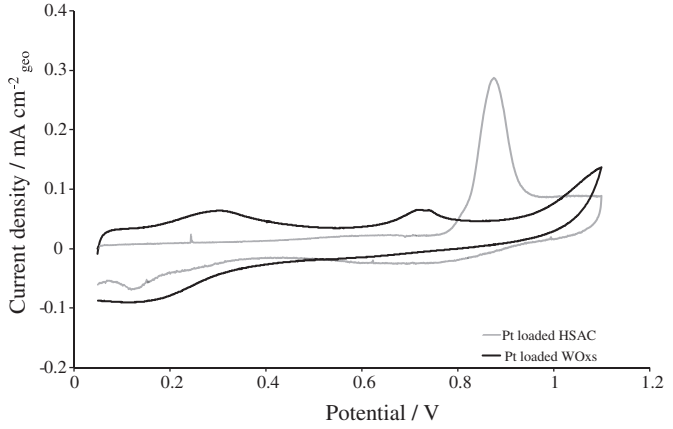

Fig. 10. CO-stripping result of Pt loaded WO_{xs} and Pt loaded HSAC with a sweep rate of 0.05 V s^{-1} in 0.1 N $HClO_4$.

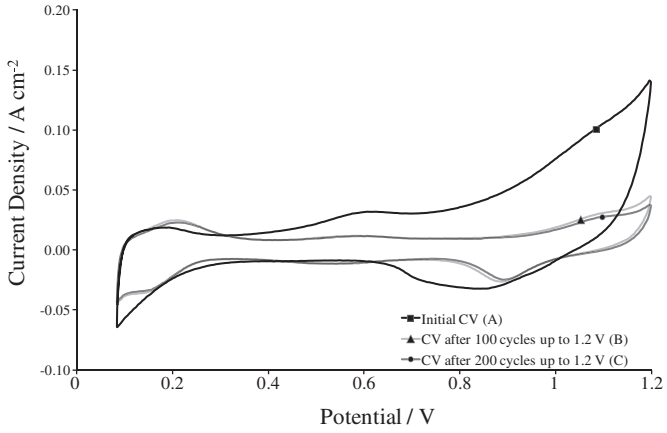

Fig. 11. In-situ CVs for HT-PEMFC of Pt/WC at different aging levels. (A) Initial scan, (B) after 100 cycles between 0.052 V and 1.2 V (C) after 100 consecutive cycles between 0.052 V and 1.2 V.

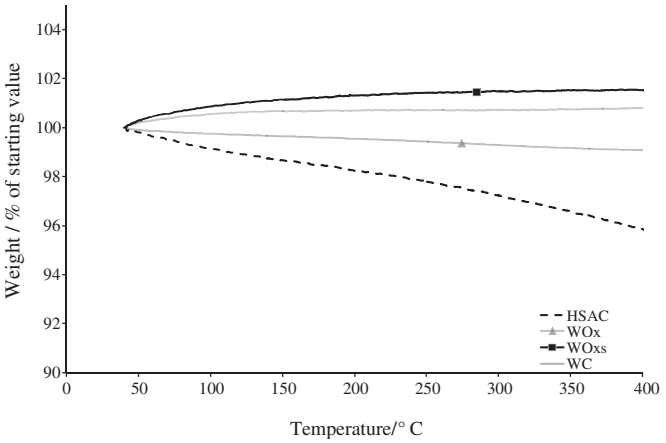

Fig. 13. TGA of WO_x, WO_{xs}, WC and HSAC from 40 °C to 400 °C at a scan rate of 10 °C s^{-1} under air atmosphere.

3.5. Potential cycling

Potential Cycling (PC) experiments were done in order to get information on the stability of the platinum loaded tungsten based support material and compared to measurements on Pt loaded HSAC. The results are shown in Fig. 7, Fig. 8 and are summarized in Fig. 9. The decrease of the H_{upd} charge (Fig. 7) of Pt/WO_{xs} can be attributed to the loss of active platinum sites. The C_{dl}, which can be seen at 0.6 V, is not changing, so the surface area and the amount of tungsten based support material is not changing significantly and no loss of support material can be observed. The loss of charge in the low potential region can be attributed to Pt-agglomeration or Pt-dissolution.

In Fig. 8 the CV scans of a PC experiment with Pt/HSAC are shown. The decrease of the H_{upd} charge (between 0.052 and 0.3 V) is much higher compared to WO_x, especially when the electrode is cycled up to potentials of 1.3 V, where almost the whole H_{upd} charge is lost after the PC.

In Fig. 9 the results of the PC experiments are summarized. Depending on the upper reverse potential the remaining H_{upd} charge in the low Potential region is calculated and compared to the starting value. The Pt loaded WO_{xs} catalyst supports showed a much higher remaining H_{upd} especially at potentials up to 1.3 V, indicating a higher stability of the catalyst and catalyst support system (compare Fig. 7).

3.6. CO-stripping

The CV curves after the adsorption of a CO monolayer were recorded in order to determine the CO-oxidation behavior of Pt on different catalyst support materials, as shown in Fig. 10. In the first scan the CO-oxidation behavior from Pt on WO_{xs} is different from the CO-oxidation behavior from Pt on carbon. The CO-oxidation peak of tungsten based supports at 0.8 V is much smaller compared to Pt on HSAC, but therefore a broader peak at lower potentials appears. In Fig. 10 a clear CO oxidation of Pt loaded WO_{xs} between 0.6 and 0.8 V is observed. It is significantly smaller than the maxima for Pt on HSAC. The calculated ECA from the CO-stripping experiments of WO_{xs} based catalyst support is only 8 m^2 g^{-1} Pt.

3.7. In-situ CV

PBI based MEAs were produced according to the procedure described in Section 2.5 in order to get information about the stability and performance of tungsten based catalyst support materials. On the working electrode WC, home-made WO_{xs} or WO_x with and without platinum were used. A Pt/HSAC electrode was used as reference electrode.

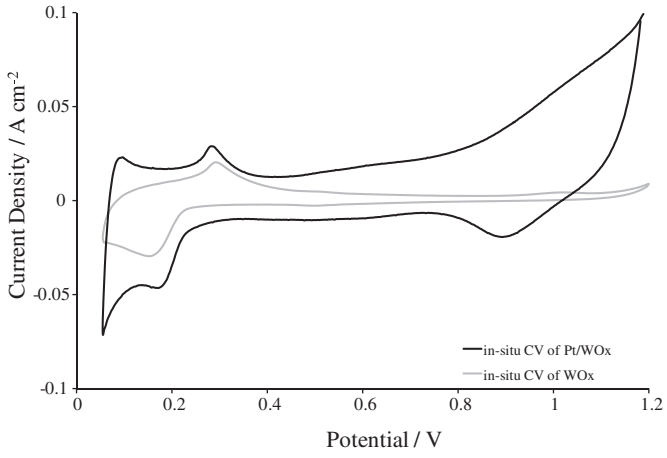

Fig. 12. In-situ CVs of WO_x with (A) and without platinum (B) on the working electrode after 100 cycles between 0.052 V and 1.2 V with a sweep rate of 0.050 V s^{-1} in 0.1 N $HClO_4$.

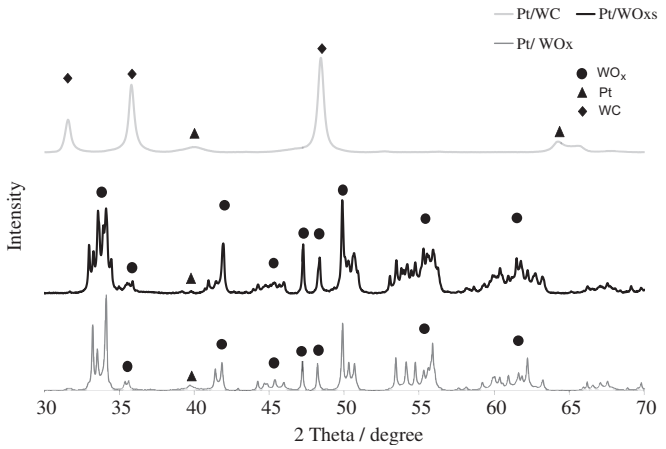

Fig. 14. XRD patterns of Pt/WC, Pt/WO_x and Pt/WO_{xs}.

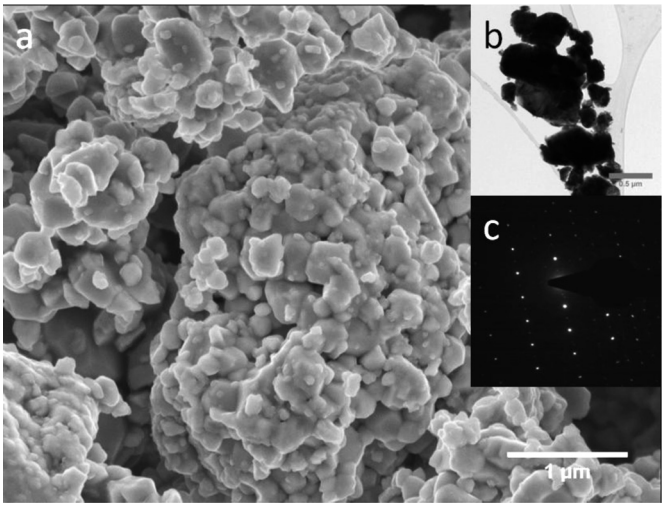

Fig. 15. (a) Secondary electron top view image shows the crystalline morphology of WO_x. (b) High-contrast TEM bright field image of WO_x particles and related electron diffraction pattern (c).

The in-situ CV for HT-PEM of a Pt/WC working electrode is presented in Fig. 11. The initial CV (A) shows a different shape in contrast to the peaks after 100 cycles between 0.052 V and 1.2 V (B). The region in the range of 0.052–0.4 V shows similarities to the character of WO_x. The cathodic oxidation region (>0.7 V) stabilizes after gradually diminishing (C), which is due to the electro-oxidation of WC–WO_x. The WO_x formation on the WC support in the range between 0.052 V and 0.4 V pretends an increase in the H_{upd} charge, when platinum loaded WC is used.

The in-situ CVs after 100 cycles of WO_x-based working electrodes with (A) and without (B) platinum are shown in Fig. 12. The cathodic peak at 0.3 V in the WO_x and Pt/WO_{xs} working electrode can be attributed to the intercalation of protons and forming hydrogen tungsten bronzes (H_xWO_3), according to equation (2). The difference between Pt/WO_{xs} and WO_x in the low potential region (<0.4 V) can be attributed to H_2 formation and its re-oxidation at the platinum catalyst.

3.8. TGA

The TGA measurements in air of WO_{xs}, WC and WO_x were done to get information about the stability of tungsten based support materials and are presented in Fig. 13.

Commercial WC possesses a stable behavior up to 400 °C under air atmosphere. In contrast to that stable behavior, the commercial WO_x shows a linear decrease of weight. The self-made WO_{xs} revealed a weight gain up to 400 °C. When compared to today's widely used HSAC support materials, the weight loss of the tungsten based materials is insignificant up to 400 °C.

The different behavior of WO_{xs} and WO_x at temperatures up to 250 °C occurs due to incomplete oxidation of WC in the synthesis of WO_{xs}. This can explain a weight gain of 2% for WC. In contrast to that, the commercial available WO_x powders are losing about 1% of the initial weight up to 250 °C, which can be explained by impurities in the fabrication process.

3.9. XRD and electron microscopy analysis

The XRD patterns for Pt loaded tungsten based catalyst support materials are given in Fig. 14. The diffractogram of the pre-treated WC shows the characteristic reflections for Pt-fcc and hexagonal WC. The procedure to synthesize Pt on self-made WO_{xs} leads to a similar, but not equal, XRD pattern compared to Pt on WO_x, which is in accordance with the *ex-situ* and *in-situ* CV results and the TGA measurement. The intensity as well as the number of reflections is changed in these two patterns indicating a change in symmetry. In all patterns, the WC, WO_x and WO_{xs} signals possess a high diffraction intensity, in contrast to the platinum signals at 39.7° and 63.5° 2θ which are rather small. In addition, the observed reflections of Pt are broad due to the small size of the Pt particles. This finding is in good accordance to the results of the HR-TEM measurements shown later.

Electron microscopy investigations were performed in order to get information on the size of the WO_x and Pt particles as well as the platinum distribution on WO_x. As an example Fig. 15 shows SEM and TEM images of untreated WO_x particles without platinum. The size of the connected WO_x particles ranges from 0.1 µm to 0.8 µm. With the aid of EDX measurements performed in the SEM a loading of 13 wt% of Pt on WO_x was confirmed. The high-contrast TEM bright field image (b) and electron diffraction pattern (c), shown as insets in Fig. 15 clarify the high crystallinity of the WO_x particles.

The catalyst particles are randomly distributed on the surface of the WO_x particles as visible in Fig. 16. The morphology of the WO_x particles is not very uniform. Nevertheless, the diameter of the platinum particles can be estimated from the high resolution micrograph (Fig. 16). It displays the characteristic Pt-interatomic distances of small spherical platinum particles in a (111) lattice plane configuration and reveals a Pt crystal size of about 3–4 nm. In Fig. 17 the Pt loaded WO_{xs} support materials are shown. The

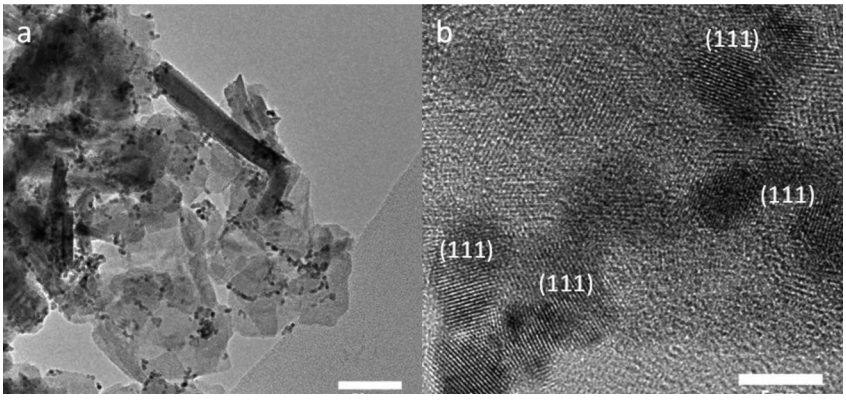

Fig. 16. TEM images of two representative areas of WO_x. 13 wt% Pt loaded WO_x (a) and detail with visible (111) lattice planes of Pt on WO_x (b).

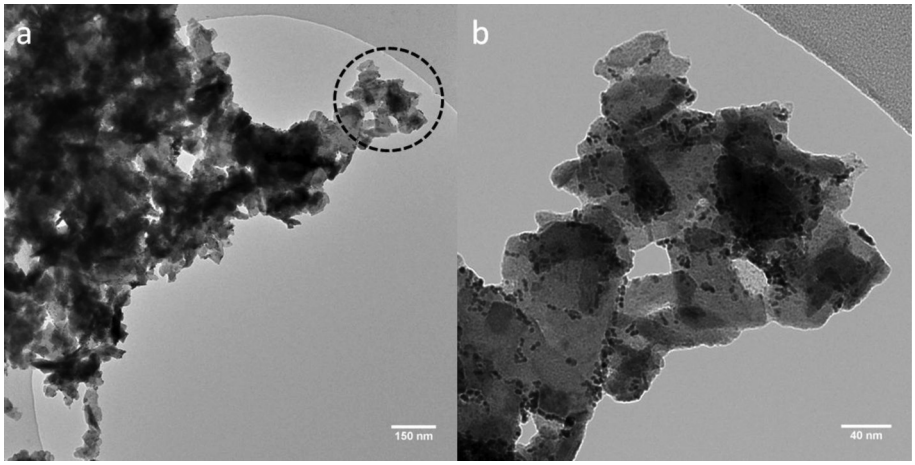

Fig. 17. TEM images of two representative areas of WO_{xs}. 13 wt% Pt loaded WO_{xs} (a) and detail of Pt on WO_{xs} (b).

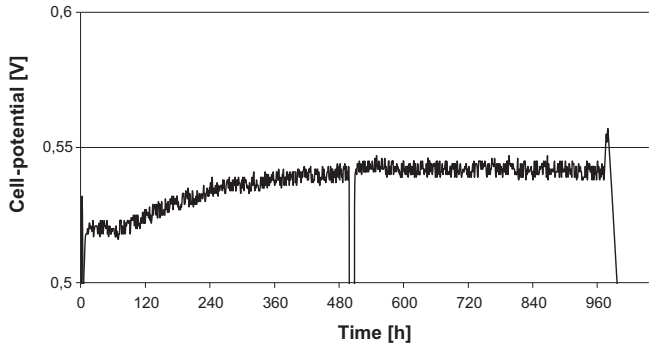

Fig. 18. 980 h test of a HT-PEM MEA in a 20-cell HT-PEMFC stack with methanol reformate on the anode at 160 °C and 0.2 A cm^{-2} current density at ambient pressure.

platinum distribution and the particle sizes of WO_{xs} are in the same range as in the WO_x samples.

3.10. HT-PEM fuel cell results

The catalyst support material was used as anode support in HT-PEM fuel cells. The WO_x-based anode was doped with phosphoric acid and pressed with a standard HSAC-cathode.

In Fig. 18 the results of a HT-PEM MEA test for 980 h with a WO_x-based anode are shown. After a conditioning time of about 500 h with rising cell potential, a stable cell potential until 980 h was obtained.

4. Conclusions

Self-made WO_{xs}, commercial available WC and commercial available WO_x were evaluated as a catalyst support material for HT-PEM fuel cells. The self-made WO_{xs} was compared to the starting material WC and commercial available WO_x. The electrochemical and chemical characteristics were determined via *ex-situ* CV, PC, TGA, SEM and TEM and *in-situ* CV and PC measurements. The chemical and electrochemical treatment and high electrochemical potentials are leading to a formation of WO_x on the surface of WC. WO_x formed during the PC leads to the formation of hydrogen tungsten bronzes and to the oxidation and reduction of sub-stoichiometric oxides. The loss or the oxidation/reduction of catalyst support material can be identified from the C_{dl} at potentials in the cathodic scan direction in the region higher than 0.7 V. WO_x and WO_{xs} were used as catalyst support material for further investigations because WC gets oxidized to WO_x under fuel cell conditions.

XRD investigations showed that the self-made WO_{xs} is formed under oxidizing acidic conditions. The commercially available WO_x shows the same electrochemical characteristics compared to the self-made WO_{xs}. The onset potential of the CO oxidation is shifted to more negative values. This effect arises from a hydrogen spill-over on the surface of WO_x, which liberates the active Pt sites from contaminants.

HT-PEM *in-situ* experiments with WC based MEAs show a comparable formation of WO_x (or hydrogen tungsten bronzes), which was confirmed with measurements of MEAs with a WO_x working electrode without Pt.

In-situ measurements show that the deposition procedure of platinum on WO_x support results in a partial reduction of WO_x, which can be re-oxidized under fuel cell conditions. WO_x-based support materials have a high chemical stability up to more than 450 °C under air. The electrochemical stability under oxidizing conditions is higher compared to Pt/HSAC. TEM measurements showed that platinum particles have an average diameter of 3–4 nm and are uniformly dispersed on the tungsten based support material. A 980 h test with reformed methanol on the anode in a PBI based HT-PEM MEA at 0.2 A cm^{-2} was done. After a conditioning time of 500 h a stable cell potential for 480 h was achieved and no degradation rate was observed. This test showed that WO_x can be used as catalyst support material for the anode in HT-PEM fuel cells.

Acknowledgment

The authors would like to thank the National Innovation Program Hydrogen and Fuel Cell Technologies for the financial support of the work. The work was partly also financially supported within the program “A3plus” by the Austrian Federal Ministry for Transport, Innovation and Technology and partly within the program “ZIM-KOOP” by the German Federal Ministry for Economy and Technology. Technical support from Steffen Schmidt and Sriram Venkatesan is gratefully acknowledged.

References

[1] W.R. Baumgartner, P. Parz, S.D. Fraser, E. Wallnöfer, V. Hacker, J. Power Sourc. 182 (2008) 413.

[2] E. Wallnöfer, M. Perchthaler, V. Hacker, G. Squadrito, J. Power Sourc. 188 (2009) 192.
[3] J.M. Planeix, N. Coustel, B. Coq, V. Brotons, P.S. Kumbar, R. Dutartre, P. Geneste, P. Bernier, P.M. Ajayan, J. Am. Chem. Soc. 116 (1994) 7935.
[4] C. Park, R.T.K. Baker, J. Phys. Chem. B 102 (1998) 5168.
[5] S. Sharma, B.G. Pollet, J. Power Sourc. 208 (2012) 96.
[6] E. Lessner, W.D. Schubert, Tungsten: Properties, Chemistry, Technology of the Element, Alloys and Chemical Compounds, Kluwer Academic, NY, 1999.
[7] B.S. Hobbs, A.C.C. Tseung, J. Electrochem. Soc. 122 (1975) 1174–1177.
[8] M.A. Butler, J. Appl. Phys. 48 (1977) 1914–1920.
[9] B.S. Hobbs, A.C.C. Tseung, Nature 222 (1969) 556.
[10] Y.J. Huang, H.H. Dai, W.S. Li, G.L. Li, D. Shu, H.Y. Chen, J. Power Sourc. 184 (2008) 348.
[11] K. Ota, A. Ishihara, S. Mitsushima, K. Lee, Y. Suzuki, N. Horibe, T. Nakagawa, N. Kamiya, J. New Mater. Electrochem. Syst. 8 (2005) 25.
[12] J. Shim, C.-R. Lee, H.-K. Lee, J.-S. Lee, E.J. Cairns, J. Power Sourc. 102 (2001) 172–177.
[13] P.J. Kulesza, L.R. Faulkner, J. Electrochem. Soc. 136 (1989) 707–713.
[14] E. Antolini, E.R. Gonzalez, Appl. Catal. B 3–4 (2010) 245–266.
[15] I. Nikolov, T. Vitanov, J. Power Sourc. 5 (1980) 273–281.
[16] I. Nikolov, T. Vitanov, J. Power Sourc. 5 (1980) 283–290.
[17] C.D.A. Brady, E.J. Rees, G.T. Burstein, J. Power Sourc. 179 (2008) 17–26.
[18] H. Chhina, S. Campbell, O. Kesler, J. Electrochem. Soc. 154 (2007) B533–B539.
[19] H. Meng, P.K. Shen, Chem. Commun. (2005) 4408–4410.
[20] H. Meng, P.K. Shen, Electrochem. Commun. 8 (2006) 588–594.
[21] H. Meng, P.K. Shen, J. Phys. Chem. B 109 (2005) 22705–22709.
[22] L.G.R.A. Santos, K.S. Freitas, E.A. Ticianelli, J. Solid State Electrochem. 11 (2007) 1541–1548.
[23] M. Shao, B. Merzougui, K. Shoemaker, L. Stolar, L. Protsailo, Z.J. Mellinger, I.H. Hsu, J.G. Chen, J. Power Sourc. 196 (2011) 7426–7434.
[24] R. Ganesan, J.S. Lee, J. Power Sourc. 157 (2006) 217–221.
[25] W. Zhu, A. Ignaszak, C. Song, R. Baker, R. Hui, J. Zhang, F. Nan, G. Botton, S. Ye, S. Campbell, Electrochim. Acta 61 (2012) 198–206.
[26] F. Wu, Y.L. Wang, C. Wu, J. Mater. Sci. Technol. 26 (2010) 705–710.
[27] A.J. Martin, A.M. Chaparro, L. Daza, J. Power Sourc. 169 (2011) 4187–4192.